Raman scattering from charge-density waves and application to polyacetylene

J. Phys. C: Solid State Phys. **19** (1986) 7291–7305. Printed in Great Britain

Raman scattering from charge-density waves and application to polyacetylene

B Horovitz†, Z Vardeny‡, E Ehrenfreund‡ and O Brafman‡

† Department of Physics, Ben-Gurion University of the Negev, Beer-Sheva, Israel

‡ Physics Department and Solid State Institute, Technion-Israel Institute of Technology, Haifa, Israel

Received 17 February 1986

Abstract. Oscillations in an electronic gap formed by a charge-density wave are described in terms of Raman-active amplitude modes. In a multi-phonon system we find the Raman shifts and their intensity ratios in terms of a parameter $\tilde{\lambda}$ which contains all effects of electron–phonon, electron–electron and electron–disorder interactions; the single assumption in the theory is the adiabatic limit. The theory is compared with data on polyacetylene where the relation of $\tilde{\lambda}$ with the electronic gap yields information on the type of disorder. For an electron–phonon system an *ab initio* calculation of the Raman cross section is given and compared with more conventional calculations.

1. Introduction

Recent interest in charge-density wave (CDW) compounds (for recent reviews see [1], [2]) led to intensive study of their Raman spectra. In particular, resonantly enhanced Raman scattering has been extensively used to study the CDW in trans-polyacetylene $(CH)_x$ [3–7]. The dependence of the Raman shifts on the exciting laser frequency ω_L or the 'dispersion' effect, was interpreted as an effect of inhomogeneity or disorder. Usually however, many assumptions are made in the theoretical analysis of the data; it is then not clear to what extent the conclusions on the type and strength of disorder can be trusted.

In this work we present a systematic method for analysing Raman data which allows for a critical test of any detailed theory. Section 2 describes the first stage of the method. We consider a CDW formed by the electron coupling with a multi-phonon system. These normal modes have frequencies ω_n^0 ($n = 1, 2, \ldots, N$) in the absence of coupling and electron–phonon couplings λ_n. The CDW is related to an electronic gap 2Δ. Assuming the adiabatic limit, i.e. $\omega_n^0 \ll 2\Delta$, we find the renormalised phonon frequencies ω_n^R which describe the CDW amplitude oscillation or the gap oscillation. These modes, known as amplitude modes [8], are active in Raman scattering. The frequencies ω_n^R as well as their intensity ratios in Raman scattering are found in terms of a parameter $\tilde{\lambda}$ which contains *all* the effects of electron–phonon, electron–electron and electron–disorder interactions. This analysis is very general—the single assumption is the adiabatic limit. This assumption is valid for half-filled band systems in general and for polyacetylene in particular.

Non-adiabatic corrections [9] involve the ratios $(\omega_n^R/2\Delta)^2$ which are ~ 0.01 in polyacetylene.

In § 3 we apply the method to polyacetylene. The dispersion effect is related to the resonance condition $\omega_L = 2\Delta$ for a maximal cross section. Thus different laser frequencies ω_L probe different subsystems with gap 2Δ and with the corresponding frequencies ω_n^R. This yields a phonon-gap relation or the functional dependence $\tilde{\lambda}(\Delta)$. In addition to the Raman satellites which shift with ω_L, there are 'primary' lines which practically do not shift, i.e. behave as in an ordered system. We define $\tilde{\lambda}_0$ and Δ_0 as the parameters for the ordered system, inferred from the primary lines. The data yields two types of behaviour: For *trans*-$(CH)_x$ $\tilde{\lambda}_0/\tilde{\lambda} = 1 - 0.37 \ln(\Delta/\Delta_0)$ while for *trans*-$(CH)_x$ mixed in *cis*-$(CH)_x$ $\tilde{\lambda}_0/\tilde{\lambda} = 1 - 1.0 \ln(\Delta/\Delta_0)$.

The next step in the method is to consider a specific model for inhomogeneity. For *trans*-$(CH)_x$ we find that inhomogeneity in a single parameter, i.e. the electron–phonon coupling λ is sufficient to explain the $\tilde{\lambda}(\Delta)$ relation [7], as well as predict ratios of Raman intensities. In contrast, models based on finite chain distribution [5, 6] require a large set of inhomogeneous parameters, i.e. the electron–phonon coupling of each mode λ_n, their frequencies ω_n^R (or equivalently ω_n^0), and the electron transfer integral. All these are assumed functions of chain length such that the $\tilde{\lambda}(\Delta)$ relation is satisfied. For *trans–cis* mixtures we find that a model with the least number of assumptions has an extrinsic symmetry breaking parameter.

An explicit form for the Raman cross section is not needed in §§ 2, 3 except for the assumption of a sharp maximum at $\omega_L = 2\Delta$. In § 4 we present an *ab initio* calculation of the Raman cross section for a one-dimensional electron–phonon model in the adiabatic and continuum limits. The calculation is performed in the somewhat unconventional spinor notation. Since this method led to some misunderstanding [10], we present it here in detail and hope that it will become accessible to a larger audience.

2. The $\tilde{\lambda}$ method—general results

Consider N phonon normal modes, which in the absence of coupling to electrons have wave-vector $\boldsymbol{q}_0$ and frequencies $\omega_n^0 (n = 1, 2, \ldots, N)$. In the presence of electron–phonon coupling a CDW is formed, i.e. the phonon amplitudes $u_n(t)$ acquire a finite expectation value. This usually requires nesting of the electron Fermi surface [11] as e.g. in a one-dimensional system. However, the mechanism and details of the CDW formation are not important in this section. The *single* assumption here is the adiabatic limit $\omega_n^0 \ll 2\Delta$, where 2Δ is the gap at the Fermi surface formed by the CDW.

The electron–phonon interaction Hamiltonian is

$$H_{\text{el-ph}} = \sum_{n=1}^{N} g_n \exp(-i\boldsymbol{q}_0 \cdot \boldsymbol{r}_0^n) u_n(t) C + \text{HC} \tag{1}$$

where g_n are coupling constants, $\boldsymbol{r}_0^n$ is a reference coordinate of the nth CDW component, and C is bilinear in electron operators which transfers momentum $\boldsymbol{q}_0$. In the following we consider only amplitude oscillations and fix the phases, i.e. choose $\boldsymbol{r}_0^n$, so that $g_n \exp(-i\boldsymbol{q}_0 \cdot \boldsymbol{r}_0^n)$ are all real. This choice maximises the interaction energy and is therefore the ground state if no other energies depend on $\boldsymbol{r}_0^n$, i.e. in an incommensurate CDW. Commensurability energies affect this choice significantly only in dimerised systems [12]. The relevant phonons then induce either a bond-centred CDW or a site-centred

CDW; relative to a bond centre these are symmetric or antisymmetric, respectively. In $(CH)_x$ there are three such symmetric modes, and one antisymmetric mode [13]. The latter is mainly a C–H stretch and its weak coupling with the π-electrons can be neglected.

We thus define the real amplitudes $\Delta_n^d(t) = g_n u_n(t) \exp(-i\boldsymbol{q}_0 \cdot \boldsymbol{r}_0^n)$ so that

$$H_{\text{el-ph}} = \Delta_d(t)[C + C^+] \tag{2}$$

and $\Delta_d(t) = \Sigma_n \Delta_n^d(t)$. The electrons respond only to this combination.

The effect of all the interactions in the system—electron–phonon, electron–electron and electron–impurity (or disorder) is given by the expectation value

$$\langle H_{\text{el}} + H_{\text{el-el}} + H_{\text{el-ph}} + H_{\text{dis}} \rangle \equiv -N(0)E_i\{\Delta_d, \dot{\Delta}_d\} \tag{3}$$

where $N(0)$ is the electron density of states at the Fermi level. The adiabatic assumption means that E_i is a function only of $\Delta_d(t)$ and not of its time derivative $\dot{\Delta}_d(t)$, i.e. the electrons follow the instantaneous value of the ion field $\Delta_d(t)$ and do not have independent dynamics.

Dynamics in this system obeys the effective Lagrangian

$$L\{\Delta_n\} = N(0)\left(\Sigma_n \frac{1}{4\lambda_n}[-(\Delta_n^d)^2 + (\dot{\Delta}_n^d/\omega_n^0)^2] + E_i(\Delta_d)\right) \tag{4}$$

where $\lambda_n = |g_n|^2 N(0)/\omega_n^0$ are dimensionless. In the ground state $\Delta_n^{d0} = 2\lambda_n E_i'(\Delta_d^0)$ where $\Delta_d^0 = \Sigma_n \Delta_n^{d0}$ and $\lambda = \Sigma_n \lambda_n$. Expanding (4) around the ground state $\Delta_n(t) = \Delta_n^{d0} + \delta_n(t)$ yields to second order in $\delta_n(t)$

$$L\{\delta_n\} = N(0)\left(\Sigma_n \frac{1}{4\lambda_n}[-\delta_n^2 + (\dot{\delta}_n/\omega_n^0)^2] + [(1 + 2\tilde{\lambda})/4\lambda]^2\right). \tag{5}$$

The central parameter in this section $\tilde{\lambda}$ is defined by

$$E_i''(\Delta_d)|_{\text{ground state}} = (1 - 2\tilde{\lambda})/2\lambda \tag{6}$$

and $\delta(t) = \Sigma_n \delta_n(t)$. In the Peierls model with no electron–electron interactions (see Appendix 1) $\tilde{\lambda} = \lambda$ and $\Delta_d = \Delta$. The equation of motion becomes

$$\delta_n(t) + \ddot{\delta}_n(t)/(\omega_n^0)^2 = (\lambda_n/\lambda)(1 - 2\tilde{\lambda})\delta(t). \tag{7}$$

A Fourier transform yields the equation for the renormalised amplitude mode frequencies $\omega = \omega_n^R$

$$D_0(\omega) = \Sigma_n(\lambda_n/\lambda)(\omega_n^0)^2/[\omega^2 - (\omega_n^0)^2] = -1/(1 - 2\tilde{\lambda}). \tag{8}$$

We are now ready to look at the Raman scattering amplitude $M(\omega_L, \omega)$, where ω_L is the incoming laser frequency and ω is the Raman shift. Radiation couples to the phonons through electrons so that $M(\omega_L, \omega) \sim \tilde{A}(\omega_L, \omega)\Sigma_n g_n u_n$ where $\tilde{A}(\omega_L, \omega)$ involves electronic transitions (an example is shown in figure 1(*b*)). For $\omega \ll \omega_L, 2\Delta$ the only ω-dependence comes from the generated phonons $\Sigma_n g_n u_n$. The cross section involves summation on all final states $|m\rangle$ whose energy E_m differs from the ground state energy E_0 by ω. This leads to

$$\sum_m |\langle m| \sum_n g_n u_n |0\rangle|^2 \, \delta(E_m - E_0 - \omega) = -\frac{1}{\pi} \operatorname{Im} D(\omega). \tag{9}$$

$D(\omega)$ is a combined phonon propagator for the renormalised phonons. One has to diagonalise the N equations (7) and find the electron–phonon coupling of each eigen-

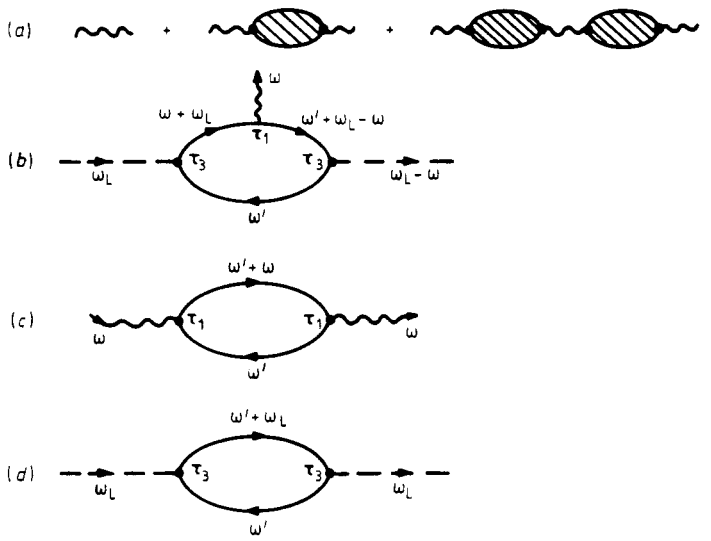

Figure 1. (*a*) Phonon renormalisation. The shaded bubble is the full mass insertion, including electron–electron and electron–disorder interactions. (*b*) Raman amplitude in the Peierls model. (*c*) The bubble of (*a*) in the Peierls model. (*d*) Conductivity diagram in the Peierls model.

function to determine $D(\omega)$. It is more convenient to use a diagramatic approach where the bare phonon propagators $2\omega_n^0/[\omega^2 - (\omega_n^0)^2]$ are renormalised by the same polarisation bubble $\pi(\omega)$. The dressed propagator is given by figure 1(*a*). Each wavy line is a sum

$$\sum_n |g_n|^2 2\omega_n^0/[\omega^2 - (\omega_n^0)^2] = 2D_0(\omega)/N(0).$$

The bubble $\pi(\omega)$ is a self-mass insertion which in general includes electron–electron and disorder interactions symbolised by the shading in figure 1(*a*). The geometric sum in figure 1(*a*) is

$$D(\omega) = \frac{2\lambda D_0(\omega)/N(0)}{1 - 2\lambda D_0(\omega)\pi(\omega)/N(0)} \xrightarrow{\omega \ll \Delta} \frac{2\lambda D_0(\omega)/N(0)}{1 + (1 - 2\tilde{\lambda})D_0(\omega)}. \tag{10}$$

For $\omega \ll 2\Delta$ $\pi(\omega)$ is independent of the phonon propagators; comparing the poles of (10) with (8) identifies $\pi(0)$ as $\pi(0) = (2\tilde{\lambda} - 1)N(0)/2\lambda$ which yields the last form in (10). In Appendix 1 we derive $\pi(\omega)$ for the Peierls model and find again that $\tilde{\lambda} = \lambda$ (A5).

The importance of equation (10) is that its residue at the pole $\omega = \omega_n^R$ is the intensity of the nth mode

$$I_n \sim \left(\frac{\partial}{\partial \omega} D_0(\omega)\right)^{-1} \qquad \text{at } \omega = \omega_n^R. \tag{11}$$

The coefficient which makes (11) an identity is independent of ω if $\omega \ll 2\Delta$, so that (11) yields intensity ratios of different modes.

Note that (9) and (11) are $(2N - 1)$ equations for the $2N$ unknowns $\tilde{\lambda}$, ω_n^0 and λ_n/λ. Additional equations can be found by studying infrared active modes [14] or by assuming a model for $\Delta(\tilde{\lambda})$.

Equations (9) and (11) become most powerful when we can change the parameter $\tilde{\lambda}$ without affecting $D_0(\omega)$. This can be achieved when only the electrons are affected. The frequencies ω_n^0 and the ratios λ_n/λ are then not affected (unlike λ); the reason for λ_n/λ being independent of $\tilde{\lambda}$ is that they represent the geometry of the non-interacting system, i.e. the projection of the nth bare normal mode on the gradient of the electron–ion potential, or bond direction in $(CH)_x$. In the next section we show that this situation applies to $(CH)_x$ through the effect of disorder.

To conclude this section we note a sum rule for $D(\omega)$. Since it is a retarded correlation function it satisfies the Kramers–Kronig relation

$$\operatorname{Re} D(\omega) = \frac{2}{\pi}\int_0^\infty \frac{\nu \operatorname{Im} D(\omega)}{\nu^2 - \omega^2}\,\mathrm{d}\nu.$$

Taking the limit $\omega \to \infty$ yields

$$\int_0^\infty \omega \operatorname{Im} D(\omega)\,\mathrm{d}\omega = -(\lambda\pi/N(0))\sum_n (\lambda_n/\lambda)(\omega_n^0)^2 \tag{12}$$

which is independent of $\tilde{\lambda}$.

Thus ratios of the integrated cross section (or total energy loss) would show more clearly the ω_L-dependence of $|\tilde{A}(\omega_L, 0)|^2$.

3. The $\tilde{\lambda}$ method—application to $(CH)_x$

In this section we apply the method of § 2 to data on *trans*-$(CH)_x$. This data is examined in detail elsewhere [15], while here we present only the main results as a demonstration of our method. We stress that the results of § 2 are extremely general—they include all interactions through a single parameter $\tilde{\lambda}$. In particular, $\tilde{\lambda}$ is affected by disorder. We claim that the bare parameters in $D_0(\omega)$ are not affected by disorder; these parameters are determined by the strongly bound σ-bonds which should not be sensitive to disorder. This is also supported by the isotope independence of $\tilde{\lambda}$ found below. The single assumption of § 2, the adiabatic limit, is very well satisfied here since $(\omega_n^R/2\Delta)^2 \sim 0.01$.

We first summarise the dispersion effect. For a given laser frequency ω_L the Raman-active modes show a primary line independent of ω_L and a satellite line which shifts to higher frequencies as ω_L increases; an example is shown in figure 2. The splitting is clear for the strongly coupled modes $n = 1$ and $n = 3$, while the $n = 2$ line does not shift sufficiently to resolve the splitting.

The dispersion effect is explained by inhomogeneity in the gap 2Δ [2–7] and by a sharp maximum in the cross section when the resonance condition $\omega_L = 2\Delta$ is satisfied (an explicit case is calculated in § 4). The primary lines correspond to a maximum in the distribution at $2\Delta_0$ and may be considered as the lines of an ordered phase [16]. The satellites correspond to subsystems whose 2Δ satisfies $2\Delta = \omega_L$. Since $\Delta = \Delta(\tilde{\lambda})$ the inhomogeneity in Δ leads to a distribution in $\tilde{\lambda}$ and hence in ω_n^R.

The data can be most efficiently analysed by the product rule. Equation (8) can be written as a polynomial in ω^2 with roots at $(\omega_n^R)^2$ so that

$$1 + (1 - 2\tilde{\lambda})D_0(\omega) = \prod_n [\omega^2 - (\omega_n^R)^2]/[\omega^2 - (\omega_n^0)^2].$$

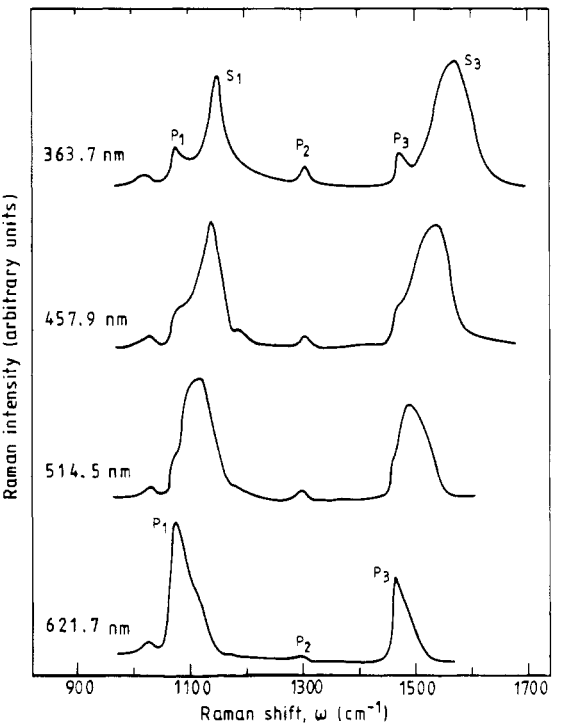

Figure 2. The dispersion effect of the resonant Raman spectra of *trans*-$(CH)_x$ at 300 K. P and S correspond to the primary and satellite position, respectively.

Comparing values at $\omega = 0$ yields the product rule

$$\prod_{n=1}^{N} (\omega_n^R/\omega_n^0)^2 = 2\tilde{\lambda}. \tag{13}$$

This equation is valid for both the satellites at frequencies ω_n^S whose $\tilde{\lambda}$ depends on ω_L, and for the primaries at frequencies ω_n^P and a fixed $\tilde{\lambda} = \tilde{\lambda}_0$. The ratio of the corresponding equations is

$$\prod_{n=1}^{N} (\omega_n^P/\omega_n^S)^2 = \tilde{\lambda}_0/\tilde{\lambda}. \tag{14}$$

This ratio is known directly from experiment and is shown in figure 3 as a function of $\ln(\omega_L)$ for *trans*-$(CH)_x$, *trans*-$(CD)_x$ and mixed *trans–cis*-$(CH)_x$.

Figure 3 exhibits a few remarkable features. First, within the accuracy of the data (14) is isotope independent. Note that individual frequencies shift by 10–20% from $(CH)_x$ to $(CD)_x$; yet the product (14) is isotope independent to within 1%. This is indeed expected from (14) since $\tilde{\lambda}$ (6) is an electronic property (λ is also isotope independent [17]). The isotope independence [17] also supports our claim that ω_n^0 are not affected by the disorder; if they were affected then figure 3 implies the unlikely result that $(\tilde{\lambda}_0/\tilde{\lambda})\Pi_n(\bar{\omega}_n^0/\omega_n^0)^2$ is isotope independent, where $\bar{\omega}_n^0$ is a disorder-affected ω_n^0.

The second remarkable feature of figure 3 is the clear difference between *trans*-$(CH)_x$

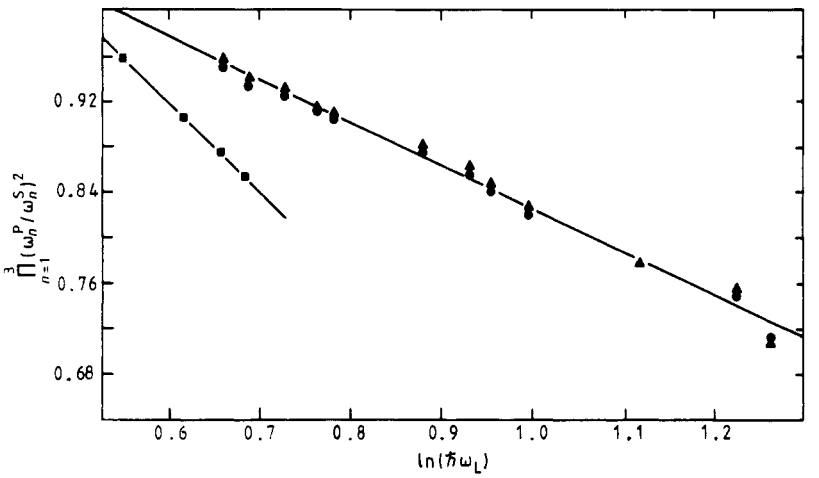

Figure 3. The $\tilde{\lambda}$-plot. The experimental product relation $\Pi_{n=1}^{3}(\omega_n^P/\omega_n^S)^2$ for *trans*-$(CH)_x$ (▲), *trans*-$(CD)_x$ (●) and *trans*- in *cis*-$(CH)_x$ (■) as a function of $\ln(\omega_L)$.

and the *trans*-$(CH)_x$ lines in a *trans–cis* mixture. The strength of disorder affects the numerical range of $\tilde{\lambda}$. Figure 3 shows however that the two systems have a different *functional* relation, i.e. they differ not only in the disorder strength, but in the *type* of disorder. Thus if the *trans–cis* mixture shows finite chain effects (as expected from the way it is prepared† and from the analysis below) then all-*trans*-$(CH)_x$ shows disorder which is *not* a finite chain effect.

The third and final remarkable feature of figure 3 is the straight-line fit. For *trans*-$(CH)_x$ $\tilde{\lambda}_0/\tilde{\lambda} = 1 - 0.37\ln(\Delta/\Delta_0)$ in the rather large available range $0.1 < \ln(\Delta/\Delta_0) < 0.7$; here $\omega_L = 2\Delta$ and $2\Delta_0$ is the intercept at $\tilde{\lambda}_0/\tilde{\lambda} = 1$. We find $2\Delta_0 = 1.72 \pm 0.02$ eV at 300 K, demonstrating a most accurate way of determining the gap in the ordered phase. For *trans–cis* mixtures we find $\tilde{\lambda}_0/\tilde{\lambda} = 1 - 1.0\ln(\Delta/\Delta_0)$ with $2\Delta_0 = 1.65$ eV at 80 K in the more limited available range of $0.1 < \ln(\Delta/\Delta_0) < 0.2$.

To exploit the method of § 2 to its full extent we need to solve for the six unknowns (five in $D_0(\omega)$ and $\tilde{\lambda}_0$) by using (8) for ω_n^R for each of the twelve available laser frequencies; there are clearly more equations than unknowns. The best fit [15] for the *trans*-$(CH)_x$ data yields $2\tilde{\lambda} = (\ln(2E_c/\Delta))^{-1}$ with $E_c = 6.3$ eV and the parameters for $D_0(\omega)$ in table 1. This relation is precisely that of the Peierls model (Appendix 1) with $\tilde{\lambda} = \lambda$. E_c is then the band width and our value is in the range of band structure estimates [18]. We thus conclude from the data that a single inhomogeneous parameter, the

Table 1. The parameters of $D_0(\omega)$ for *trans*-$(CH)_x$ and $(CD)_x$ at 300 K.

	trans-$(CH)_x$	*trans*-$(CD)_x$
$\omega_n^0(10^3\ \mathrm{cm}^{-1})$	1.23 1.31 2.04	0.92 1.21 2.04
λ_n/λ	0.07 0.02 0.91	0.06 0.005 0.93

† *cis*-$(CH)_x$ is transformed into *trans*-$(CH)_x$ by heating. By restricting the heating time, segments of the *trans*-isomer are formed within a *cis*-matrix.

electron–phonon coupling λ, is sufficient to explain the data. This and other possible interpretations are further discussed in § 5.

The function $D_0(\omega)$ (table 1) and the values of $\tilde{\lambda}$ can be tested by evaluating ratios of Raman intensities according to (10). As apparent in figure 2 the intensity ratio I_3/I_1 increases with ω_L from 3.8 at $\omega_L = 2.0$ eV to 7.0 at $\omega_L = 3.4$ eV. The non-trivial dependence of I_3/I_1 on ω_L is shown in figure 4 together with the theoretical prediction of (11). The striking agreement in figure 4 confirms the validity of our method. The function $D_0(\omega)$ was also tested by predicting with equal success the infrared activity induced by either doping or by photogeneration [7, 14].

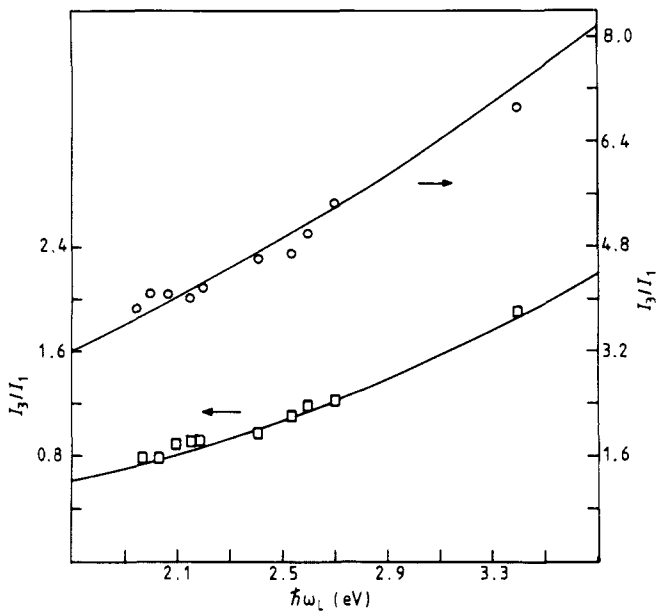

Figure 4. The ratios I_3/I_1 for *trans*-$(CH)_x$ (□) and *trans*-$(CD)_x$ (○) as a function of ω_L.

We include in this section an interesting property of the lineshapes. When the bare modes are sharp (small natural or 'bare' linewidth) the lineshape is determined by the distribution in $\tilde{\lambda}$, $P(\tilde{\lambda})$. The cross section has then the form ($\omega \ll \omega_L$)

$$\int d\tilde{\lambda}\, |\tilde{a}(\omega_L; \Delta(\tilde{\lambda}))|^2\, P(\tilde{\lambda})\, \mathrm{Im}[1 + D_0^{-1}(\omega) - 2\tilde{\lambda}]^{-1} = \tfrac{1}{2}F[(1 + D_0^{-1}(\omega))/2] \qquad (15)$$

since the $\tilde{\lambda}$-integration involves the pole at $2\tilde{\lambda} = 1 + D_0^{-1}(\omega)$ and $F(x) = \pi|\tilde{A}[\omega_L, \Delta(x)]|^2 P(x)$. Here $\tilde{A}(\omega_L; \Delta) = \tilde{A}(\omega_L, \omega = 0)$ also displays the dependence on Δ. Thus the ω-dependence is contained in the combination $1 + D_0^{-1}(\omega)$. A maximum in $F(x)$ at x_m determines three solutions for ω_n^R. The unusual feature is that the value of $F(x_m)$ is *common* to the three solutions. Thus all Raman lines (with small natural linewidth) have equal heights and the difference in intensity is contained in their widths. This feature is indeed apparent in the data of figure 2. Note also that if the amplitude $\tilde{A}(\omega_L; \Delta)$ is known from theory then the distribution $P(\tilde{\lambda})$ can be determined from $F(x)/|\tilde{A}[\omega_L, \Delta(x)]|^2$.

A similar analysis for the *trans–cis* mixture has shown [7] that the $\tilde{\lambda}(\Delta)$ relation is consistent with a Peierls model which includes an additive energy term $b\Delta$, where b

measures the disorder strength. The linear dependence on Δ means that the $\Delta \rightarrow -\Delta$ symmetry is broken. This is possible in finite chains by either end effects or by interaction with the *cis* chains where the symmetry is already broken.

To conclude this section we emphasise again the generality of the $\tilde{\lambda}$-method. Details of the amplitude $\tilde{A}(\omega_L, \Delta)$ were not required except for the general property that it has a maximum at resonance, $\omega_L = 2\Delta$. Thus the analysis was done without any *a priori* assumption on the electron–electron interaction, electron–disorder interaction and even the dimensionality of the system. The parameters of $D_0(\omega)$ and $\tilde{\lambda}$ were *derived* from the data. It is only in the final step of identifying the $\tilde{\lambda}(\Delta)$ relation that a specific model is suggested. A model with a minimal set of assumptions is that of an inhomogeneous electron–phonon coupling in *trans*-$(CH)_x$ and an inhomogeneous symmetry breaking parameter b in the *trans–cis* mixture.

4. The Raman cross section

In this section we present an *ab initio* calculation of the Raman cross section in the continuum adiabatic Peierls model, i.e. $\omega_n^R \ll 2\Delta \ll 2E_c$ with only the electron–phonon interaction in one dimension (E_c is approximately the band width). We use the somewhat unconventional spinor notation so that we occasionally compare results with other methods.

In the continuum limit one can define independent right and left moving electrons

$$C_{1,k} = C_{k+k_F} \qquad C_{2,k} = C_{k-k_F} \qquad |k| \ll k_F$$

since only states near the Fermi points $\pm k_F$ are important. The electron dispersion is $\pm v_F k$ near the Fermi points and v_F is the Fermi velocity. The electron Hamiltonian is then

$$H_e = \sum_k v_F k (C_{1,k}^\dagger C_{1,k} - C_{2,k}^\dagger C_{2,k}) = \sum_k v_F k \psi_k^\dagger + \tau_3 \psi_k \tag{16}$$

where $\psi_k^\dagger = (C_{1,k}^\dagger, C_{2,k}^\dagger)$ is a spinor and τ_i are Pauli matrices. The electron–phonon coupling (2) couples the right and left moving electrons

$$H_{el\text{-}ph} = \Delta \sum_k C_{1,k}^\dagger C_{2,k} + \text{HC} = \Delta \sum_k \psi_k^\dagger + \tau_1 \psi_k \tag{17}$$

Here $\Delta = \Delta_d$ since (16) and (17) can be easily diagonalised with energy eigenvalues $\pm(v_F^2 k^2 + \Delta^2)^{1/2}$ i.e. 2Δ is indeed the gap. Since conventional methods [5, 6] work with the eigen-operators $\alpha_{1,k}$, $\alpha_{2,k}$ for $\Delta \neq 0$ it is useful to exhibit them explicitly. The algebra is the same as for the Bogoliubov transformation in the theory of superconductivity [17] and yields

$$\begin{aligned} C_{1,k} &= u_k \alpha_{1,k} + v_k \alpha_{2,k} \\ C_{2,k} &= -v_k \alpha_{1,k} + u_k \alpha_{2,k} \end{aligned} \tag{18}$$

where

$$u_k^2 = (1 + v_F k / E_k)/2 \qquad v_k^2 = (1 - v_F k / E_k)/2 \tag{19}$$

and $E_k = +(v_F^2 k^2 + \Delta^2)^{1/2}$. It is now easy to check that (16, 17) are diagonalised

$$H_{el} + H_{el\text{-}ph} = \sum_k E_k (\alpha_{1,k}^\dagger \alpha_{1,k} - \alpha_{2,k}^\dagger \alpha_{2,k}). \tag{20}$$

Oscillations in Δ couple by (17) to $\Sigma_k C^+_{1,k} C_{2,k}$ which can be written in terms of $\alpha_{1,k}$, $\alpha_{2,k}$. For instance, the coupling g_n^{ex} of the mode $u_n(t)$ in the excited electronic state $\alpha_{2,k}$ is k-dependent

$$g_n^{ex}(k) = 2g_n u_k v_k = g_n(1 - v_F^2 k^2/E_k^2)^{1/2}. \tag{21}$$

This k-dependence is similar to that in the conventional approach [6, 10] for $v_F k \ll \Delta$.

We proceed to evaluate the Raman cross section in terms of the original fields ψ_k which we find more convenient. The electron current operator is the difference between right and left moving densities so that the interaction with radiation is

$$(2\pi\hbar/\omega_i)^{1/2} e v_F \sum_k \psi_k^+ \tau_3 \psi_k \sin\theta$$

where the square root is normalisation to one photon, ω_i is the photon frequency and θ is the angle between the light propagation and the chain axis.

As with the spinor notation for superconductivity [17] we can use the standard Green function perturbation theory. The electron propagator from [16, 17] is

$$G(\omega, k) = [\omega - \varepsilon\tau_3 - \Delta\tau_1]^{-1} = \frac{\omega + \varepsilon\tau_3 + \Delta\tau_1}{\omega^2 - \varepsilon^2 - \Delta^2 + i\delta} \tag{22}$$

where $\varepsilon = v_F k$ and $\delta \to +0$. The Raman amplitude in the adiabatic limit is given by the single diagram of figure 1(b). Additional (virtual) phonon excitation results in corrections of order $(\omega_n^R/2\Delta)^2$ [9]. Each full curve in figure 1(b) is the 2×2 matrix $G(\omega, k)$, the wavy line is the excited phonon and the broken lines are photons. The diagram is defined as $N(0)A(\omega_L, \omega)/\Delta$ so that A is dimensionless. Incoming light polarised parallel to the chain has an amplitude for scattering into angle θ

$$M(\omega_L, \omega) = v_F^2 e^2 (2\pi\hbar N(0)/\Delta)[\omega_L(\omega_L - \omega)]^{-1/2} \sin\theta\, A(\omega_L, \omega) \sum_n g_n u_n. \tag{23}$$

The transition rate from $|0\rangle$ to state $|m\rangle$ is from the golden rule

$$(2\pi/\hbar)|\langle m|M|0\rangle|^2 \delta(E_m - E_0 - \omega).$$

The cross section with a final state density $q^2 dq d\Omega/(2\pi)^3$ ($cq = \omega_L - \omega$, Ω is the solid angle) per incoming flux ($=c$) is then

$$\frac{d^2\sigma}{d\Omega\, d\omega} = \frac{\omega_L - \omega}{\omega_L} \frac{r_0^2}{b^2} \frac{4\lambda}{\pi^2} \frac{m v_F^3}{\Delta^2} |A(\omega_L, \omega)|^2 \sin^2\theta \operatorname{Im} \frac{-D_0(\omega)}{1 - 2\lambda D_0(\omega)\pi(\omega)/N(0)}. \tag{24}$$

Here $r_0 = e^2/mc^2$ is the electron radius, m is its mass, $N(0) = 2/(\pi v_F b^2)$, b^2 is the area per chain and (9, 10) were used. The polarisation $\pi(\omega)$ is derived in Appendix 1 and for $\omega \ll 2\Delta$ we can use $\pi(0) = (2\lambda - 1)N(0)/2\lambda$.

From figure 1(b) we have

$$N(0)A(\omega_L, \omega)/\Delta = 2i \sum_{\omega', k} \mathrm{Tr}[G(\omega', k)\tau_3\, G(\omega_L + \omega', k)\tau_1 G(\omega_L + \omega' - \omega, k)\tau_3] \tag{25}$$

with two for spin summation. The summation can be evaluated exactly in the relevant limit $\omega \ll 2\Delta$ (see Appendix 2) where $A(\omega_L, 0)$ is a function of the ratio $\omega_L/2\Delta$,

$A(\omega_L, 0) = f(\omega_L/2\Delta)/2$ with

$$f(x) = \begin{cases} \dfrac{1}{x^2-1} + \dfrac{1-2x^2}{x(1-x^2)^{3/2}} \tan^{-1} \dfrac{x}{(1-x^2)^{1/2}} & x < 1 \\ \dfrac{1}{x^2-1} + \dfrac{2x^2-1}{2x(x^2-1)^{3/2}} \left(\ln \dfrac{x-(x^2-1)^{1/2}}{x+(x^2-1)^{1/2}} + \pi i \right) & x > 1 \end{cases} \tag{26}$$

so that

$$\frac{d^2\sigma}{d\Omega\, d\omega} = \frac{\lambda r_0^2 m^2 v_F^3}{\pi^2 b^2 \Delta^2} |f(\omega_L/2\Delta)|^2 \operatorname{Im} \frac{-D_0(\omega)}{1+(1-2\lambda)D_0(\omega)}. \tag{27}$$

Equation (26) holds for $\omega \ll 2\Delta$ but also $\omega \ll |\omega_L - 2\Delta|$ so that very near resonance ($x = 1$) the singularity becomes weaker if $\omega \neq 0$.

The function $f(x)$ can be more easily evaluated by considering a derivative of the conductivity $\sigma_0(\omega_L)$ [19]. Since an amplitude mode is a modulation of Δ, $f(x)$ should be proportional to $\partial\sigma_0(\omega)/\partial\Delta$. By using the result in Appendix 1 (A1.8) we easily find that

$$\frac{\partial^2 \sigma_0(\omega_L, \Delta)}{\partial \Delta} \sim f(\omega_L/2\Delta)/\Delta \tag{28}$$

which confirms (26).

In figure 5 we show the cross section using (26) and averaged as in (15) [$|\tilde{A}|^2 = \lambda|f|^2/\Delta^2$] with a λ-distribution around $\lambda = 0.185$ and width $\Delta\lambda/\lambda = 0.03$ for $\omega_L/2\Delta_0 = 1$. Note the feature of equal heights discussed in § 3. The theoretical spectrum in figure 5 is in good agreement with the data of *trans*-$(CD)_x$ for the red excitation ($\omega_L = 1.9$ eV). Examples with higher excitation frequencies show the satellites [7, 15]. Also is shown the function $D_0(\omega)$ with the intercepts for $\lambda = 0.185$ which yield the frequencies ω_n^R at the peaks. The integrated cross section (per unit cell) can also be estimated for $(CH)_x$

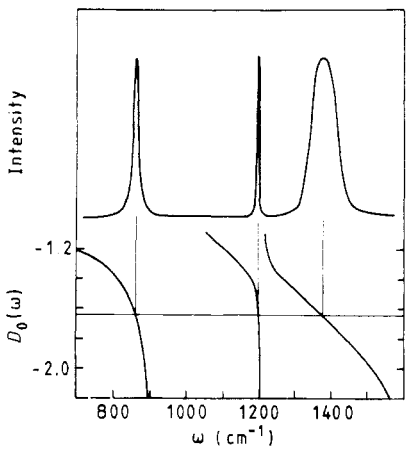

Figure 5. Theoretical Raman cross section for a three-oscillator inhomogeneous system and the function $D_0(\omega)$ with the intensity in arbitrary units. The excitation energy ω_L is chosen such that the corresponding value of $\tilde{\lambda}$ is at the peak of the distribution $P(\tilde{\lambda})$.

with the result $\sigma \sim 0.5 \times 10^{-25}|f(x)|^2$ cm^2. Comparison with data [20] shows a reasonable enhancement of $|f(x)|^2 \simeq 50$.

We note that $|f(x)|^2$ in (26) diverges as $|1-x|^{-3}$ near the resonance $x = 1$. This strong divergence is suppressed by a finite Raman frequency (A2.4) and more significantly by inter-chain coupling $t_\perp$. The latter affects $f(x)$ for $|\omega_L - 2\Delta| \lesssim t_\perp$ which for $(CH)_x$ is $|x-1| < 0.1$ [18]. Still, $|f(x)|^2$ is much sharper than the conventional expressions [5, 6, 10]. Therefore, the distribution $P(\tilde{\lambda})$ that is needed to fit the data is much narrower in our case and a double-peaked distribution [6] is not required [7].

The present formulation applies also to CDW systems with an extrinsic gap component Δ_e [21] as in *cis*-$(CH)_x$ or polythiophene. In this case $\Delta = \Delta_e + \Delta_d$, λ in (27) is replaced by $\tilde{\lambda}$ as in (10) and $\tilde{\lambda}$ is given by (6).

5. Discussion

The fundamental issue in the Raman data of $(CH)_x$ is to understand its implication on the nature of disorder. Previous theories explained the data by a distribution $P(N_c)$ in chain length or in conjugation length (CL) [3–6]. There are a number of difficulties with this approach for *trans*-$(CH)_x$: (i) A large set of assumed inhomogeneous or N_c-dependent parameters is required. $\lambda_n(N_c)$, $\beta(N_c)$ (β is the transfer integral) and $\omega_n^R(N_c)$ (which imply $\omega_n^0(N_c)$) for $n = 1, 3$ ($n = 2$ mode is usually neglected). All these assumed relations combine to yield the $\tilde{\lambda}(\Delta)$ plot, i.e. the straight line in figure 3. (ii) As figure 3 shows, the *type* of disorder is different in *trans*-$(CH)_x$ from *trans–cis* mixtures, i.e. a different distribution $P(N_c)$ cannot explain this difference within the CL model.

In contrast, we show that a *single* inhomogeneous parameter, the electron–phonon coupling λ, is sufficient to explain the $\tilde{\lambda}(\Delta)$ relation. Thus λ is the most sensitive parameter to impurities and disorder. Furthermore we have shown that the *trans–cis* mixture data does describe finite chain effects [7]. Thus, all-*trans*-$(CH)_x$ is indeed different.

It is interesting to note that the presence of a weak or even intermediate strength electron–electron interaction does not affect the above conclusions [22]. The reason is that these interactions affect only the $\ln^2(\Delta/\Delta_0)$ term in the $\tilde{\lambda}(\Delta)$ relation which is rather small. The leading $\ln(\Delta/\Delta_0)$ is the same as in the Peierls model. We have also examined the effect of disorder on both λ and electron–electron couplings [15]. The $\tilde{\lambda}$-plot (figure 3) then yields a small upper bound for the $\ln^2(\Delta/\Delta_0)$ term, resulting in a range of values (0.08 to 0.185) for λ and moderate values for the electron–electron coupling.

Besides this fundamental issue, a number of technical misunderstandings of our method appeared [10]. It was claimed that: (i) We neglect the k-dependence of the electron–phonon coupling in the excited state—this is not the case as (21) shows. (ii) We do not distinguish λ in the Raman process from λ which renormalises the frequencies ω_n^0—λ is indeed only part of the different matrix elements which define figure 1(*b*) and 1(*c*). (iii) We use 'bare' parameters of the undimerised state, while a metal–semiconductor phase transition was never observed in polyacetylene. This is precisely the elegance of our method which allows us to need very few parameters. The phase transition should appear at a temperature $\sim\Delta/k_B$ where polyacetylene does not survive. This however is completeley irrelevant to our method which is independent of when or where Δ is formed.

In conclusion we have shown a method for analysing Raman data from a CDW. The

first step is to find a phonon-gap relation, i.e. a $\tilde{\lambda}$-plot. To vary $\tilde{\lambda}$ or Δ one can use disorder but also temperature or pressure. The second step is to test theoretical models against the $\tilde{\lambda}$-plot. If a suitable model is found, then a more detailed derivation of the cross section in that model is needed for a final detailed test. This procedure was applied here successfully on *trans*-$(CH)_x$ and led us to new insights on the nature of this material.

Appendix 1. The Peierls model

In this Appendix we collect a number of well known results on the Peierls type CDW i.e. no electron–electron interactions. First note that $2\Delta_d = 2\Delta$, or the dimerisation gap equals the actual electronic gap. This follows directly from the eigenvalues of (16) and (17) $\pm E_k = \pm(v_F^2 k^2 + \Delta^2)^{1/2}$ with a gap of 2Δ. The electronic energy (3) is here

$$E_i(\Delta) = \frac{1}{N(0)}\left(\sum_k E_k - \sum_k v_F k\right) = \tfrac{1}{4}\Delta^2 + \tfrac{1}{2}\Delta^2 \ln(2E_c/\Delta) \tag{A1.1}$$

where E_c is a cut-off energy, $2E_c = 2v_F k_F \sim$ the band width and $E_c \gg \Delta$. The ground state in (4) is $\Delta = 2\lambda E_i'(\Delta)$ or $\Delta = 2E_c \exp(-1/2\lambda)$. Phonons are determined by $E_i''(\Delta)$ at the ground state (6) so that

$$\tilde{\lambda} = \lambda. \tag{A1.2}$$

We next calculate the polarisation $\pi(\omega)$ which renormalises the phonon frequencies in figure 1(*a*). In the Peierls model $\pi(\omega)$ is the single bubble of figure 1(*c*) with τ_1 in the vertices (17).

$$\pi(\omega) = \mathrm{i} \sum_{\omega', k} \mathrm{Tr}[\tau_1\, G(\omega', k)\, \tau_1\, G(\omega' + \omega, k)]. \tag{A1.3}$$

Using (22) and integrating ω' yields

$$\pi(\omega) = -2N(0) \int_{-E_c}^{E_c} \mathrm{d}\varepsilon \frac{\Delta^2 - E^2}{E(\omega^2 - 4E^2)} \tag{A1.4}$$

where $\varepsilon = v_F k$ and $E = (\varepsilon^2 + \Delta^2)^{1/2}$. For $\omega \ll 2\Delta$ we use $\int \mathrm{d}\varepsilon/E = 1/\lambda$ from the ground-state equation and the convergent integral $\int \mathrm{d}\varepsilon E^{-3/2} = 2/\Delta^2$ to find

$$\pi(0) = (2\lambda - 1)\, N(0)/2\lambda. \tag{A1.5}$$

Using (10) confirms again that $\tilde{\lambda} = \lambda$.

Finally we calculate the electronic conductivity $\sigma_0(\omega)$ (excluding the phase mode contribution [8]). This conductivity is related to the Raman cross section (26). With the current operator $ev_F \psi^+(x)\tau_3\psi(x)$ we need the correlation function, (figure 1(*d*))

$$F(\omega) = \mathrm{i} \sum_{\omega', k} \mathrm{Tr}[\tau_3\, G(\omega', k)\, \tau_3\, G(\omega' + \omega, k)]$$

$$= -N(0) \int \mathrm{d}\varepsilon \frac{2\Delta^2}{E(4E^2 - (\omega + \mathrm{i}\delta)^2)} \equiv -N(0)\, g(\omega/2\Delta). \tag{A1.6}$$

The integral converges so that $E_c \to \infty$ is allowed and

$$g(x) = \begin{cases} \dfrac{1}{x(1-x^2)^{1/2}} \tan^{-1} \dfrac{x}{(1-x^2)^{1/2}} & x < 1 \\ \dfrac{1}{2x(x^2-1)^{1/2}} \left(\ln \dfrac{x-(x^2-1)^{1/2}}{x+(x^2-1)^{1/2}} + \pi i \right) & x > 1. \end{cases} \tag{A1.7}$$

The conductivity is then [8]

$$\sigma(\omega) = \frac{\omega_p^2}{4\pi i \omega} [g(\omega/2\Delta) - 1] \tag{A1.8}$$

where $\omega_p = [4\pi e^2 v_F^2 N(0)]^{1/2}$ is the plasma frequency.

Appendix 2. The Raman amplitude

We evaluate here (25) with the Green function (22). After taking the trace the amplitude A has the form

$$A(\omega_L, \omega) = (4\Delta^2/N(0)) \sum_k [B_1(k, \omega_L, \omega) + (4v_F^2 k^2 - \omega_L^2 + \omega_L, \omega) B_2(k, \omega_L, \omega)] \tag{A2.1}$$

where $E^2 = v_F^2 k^2 + \Delta^2$ and

$$B_1(k, \omega_L, \omega) = i \sum_{\omega'} [\omega'^2 - E^2 + i\delta]^{-1} [(\omega' - \omega)^2 - E^2 + i\delta]^{-1}$$

$$B_2(k, \omega_L, \omega) = i \sum_{\omega'} [\omega'^2 - E^2 + i\delta]^{-1} [(\omega' + \omega_L)^2 - E^2 + i\delta]^{-1} \times [(\omega' + \omega_L - \omega)^2 - E^2 + i\delta]^{-1}.$$

Integrating B_1 involves the poles at $\omega' = -E + i\delta$ and $\omega' = -E + \omega + i\delta$ so that

$$B_1(k, \omega_L, \omega) = [E(\omega^2 - 4E^2 + i\delta)]^{-1}.$$

To integrate B_2 we use a Feynman trick

$$B_2(k, \omega_L, \omega) = 2i \sum_{\omega'} \int_0^1 dz_1 \int_0^{1-z_1} dz_2 [z_1(\omega'^2 - E^2 + i\delta) + z_2((\omega' + \omega_L)^2 - E^2 + i\delta) + (1 - z_1 - z_2)((\omega' + \omega_L - \omega)^2 - E^2 + i\delta)]^{-3}. \tag{A2.2}$$

We define $\tilde{\omega} = \omega' + \omega_L(1 - z_1) - \omega(1 - z_1 - z_2)$ and

$a = \Delta^2 - \omega_L^2 z_1(1 - z_1) + 2\omega\omega_L z_1(1 - z_1 - z_2) - \omega^2(1 - z_1 - z_2)(z_1 + z_2) - i\delta$

so that ($\varepsilon = v_F k$)

$$B_2 = 2 \int_0^1 dz_1 \int_0^{1-z_1} dz_2 \, i \frac{1}{2\pi} \int d\tilde{\omega} [\tilde{\omega}^2 - a - \varepsilon^2]^{-3}$$

$$= \tfrac{3}{8} \int_0^1 dz_1 \int_0^{1-z_1} dz_2 (a + \varepsilon^2)^{-5/2}. \tag{A2.3}$$

For $\mathrm{Re}(a+\varepsilon^2)<0$ the square root is $-\mathrm{i}|a+\varepsilon^2|^{-1/2}$ so that the integrand is continuous at $a+\varepsilon^2=0$. The k-integration can now be done using

$$\int \mathrm{d}\varepsilon \varepsilon^2 (a+\varepsilon^2)^{-5/2} = \tfrac{2}{3}a \qquad \int \mathrm{d}\varepsilon (a+\varepsilon^2)^{-5/2} = 4/3a^2$$

where the integration limits are $\pm\infty$ for these convergent integrals. Therefore,

$$A(\omega_\mathrm{L},\omega) = \int_{-\infty}^{\infty} \frac{\Delta^2\,\mathrm{d}\varepsilon}{E(\omega^2-4E^2+\mathrm{i}\delta)} + \Delta^2 \int_0^1 \mathrm{d}z_1 \int_0^{1-z_1} \mathrm{d}z_2 \left(\frac{1}{a} - \frac{\omega_\mathrm{L}(\omega_\mathrm{L}+\omega)}{2a^2}\right) \tag{A2.4}$$

This is exact for any ω. In the limit $\omega \ll 2\Delta$, ω_L, $|\omega_\mathrm{L}-2\Delta|$ we obtain for $A(\omega_\mathrm{L},0) = f(\omega_\mathrm{L}/2\Delta)/2$

$$f(\omega_\mathrm{L}/2\Delta) = -1 + \Delta^2 \int_0^1 \mathrm{d}z(1-z)[(2/a) - (\omega_\mathrm{L}^2/a^2)] \tag{A2.5}$$

where now $a = \Delta^2 - \omega_\mathrm{L}^2 z(1-z) - \mathrm{i}\delta$. The z-integration is straightforward with the result in (26).

References

[1] *Proc. Int. Conf. Synthetic Metals (Abano Terme) 1985: Mol. Cryst. Liq. Cryst.* **117–121**
[2] *Proc. Conf. Charge Density Waves in Solids (Budapest) 1985 in Springer Lecture Notes in Physics* vol 217 (Berlin: Springer)
[3] Harada I, Furukawa Y, Tasumi M, Shirakawa H and Ikeda S 1980 *J. Chem. Phys.* **73** 4746
[4] Lichtman L S, Sarhangi A and Fitchen D B 1979 *Solid State Commun.* **29** 191; 1980 *Solid State Commun.* **36** 869
[5] Kuzmany H, Imhoff E A, Fitchen D B and Sarhangi A 1982 *Phys. Rev.* B **26** 7109
[6] Brivio G P and Mulazzi E 1984 *Phys. Rev.* B **30** 876
[7] Vardeny Z, Ehrenfreund E, Brafman O and Horovitz B 1983 *Phys. Rev. Lett.* **51** 2326; 1985 *Phys. Rev. Lett.* **54** 75; 1984 *Syn Metals* **9** 215
[8] Lee P A, Rice T M and Anderson P W 1974 *Solid State Commun.* **14** 703
[9] Brazovskii S A and Dzyaloshinskii I E 1976 *Zh. Eksp. Teor. Fiz.* **71** 2338 (1976 *Sov. Phys.–JETP* **44** 1233)
[10] Tiziani R, Brivio G P and Mulazzi E 1985 *Phys. Rev.* B **31** 4015
Mulazzi E and Brivio G P 1984 *Mol. Cryst. Liq. Cryst.* **105** 233
[11] Horovitz B, Gutfreund H and Weger M 1975 *Phys. Rev.* B **12** 3174
[12] Horovitz B and Krumhansl J A 1984 *Phys. Rev.* B **29** 2109
[13] Schugerl F B and Kuzmany H 1981 *J. Chem. Phys.* **74** 953
[14] Horovitz B 1982 *Solid State Commun.* **41** 729
[15] Ehrenfreund E, Vardeny Z, Brafman O and Horovitz B 1986 *Phys. Rev.* B submitted for publication
[16] Yaacobi Y 1985 private communication
[17] Schrieffer J R 1964 *Theory of Superconductivity* ed. D Pines (New York: Benjamin)
[18] Grant P M and Batra I P 1983 *J. Physique Coll.* **44** C3 437
Ashkenazi J, Ehrenfreund E, Vardeny Z and Brafman O 1985 *Mol. Cryst. Liq. Cryst.* **117** 193
[19] Chantry G W 1971 in *The Raman Effect* ed. A Anderson (New York: Dekker) p 49
[20] Lauchlan L, Chen S P, Etemad S, Kletter M, Heeger A J and MacDiarmid A G 1983 *Phys. Rev.* B **27** 2301
[21] Brazovskii S and Kirova N 1981 *Zh. Eksp. Teor. Fiz. Pis.* **33** 6 (1981 *JETP Lett.* **33** 4)
[22] Horovitz B and Solyom J 1985 *Phys. Rev.* B **32** 2681